

# A New Test of Copper and Zinc Abundances in Late-Type Stars Using Ultraviolet Cu II and Zn II Lines\*

IAN U. ROEDERER<sup>1,2</sup> AND PAUL S. BARKLEM<sup>3</sup>

<sup>1</sup>*Department of Astronomy, University of Michigan, 1085 S. University Ave., Ann Arbor, MI 48109, USA*

<sup>2</sup>*Joint Institute for Nuclear Astrophysics – Center for the Evolution of the Elements (JINA-CEE), USA*

<sup>3</sup>*Theoretical Astrophysics, Department of Physics and Astronomy, Uppsala University, Box 516, SE-751 20 Uppsala, Sweden*

(Accepted for publication in the *Astrophysical Journal*)

## ABSTRACT

We present new abundances derived from Cu I, Cu II, Zn I, and Zn II lines in six warm ( $5766 \leq T_{\text{eff}} \leq 6427$  K), metal-poor ( $-2.50 \leq [\text{Fe}/\text{H}] \leq -0.95$ ) dwarf and subgiant ( $3.64 \leq \log g \leq 4.44$ ) stars. These abundances are derived from archival high-resolution ultraviolet spectra from the Space Telescope Imaging Spectrograph on board the *Hubble Space Telescope* and ground-based optical spectra from several observatories. Ionized Cu and Zn are the majority species, and abundances derived from Cu II and Zn II lines should be largely insensitive to departures from local thermodynamic equilibrium (LTE). We find good agreement between the  $[\text{Zn}/\text{H}]$  ratios derived separately from Zn I and Zn II lines, suggesting that departures from LTE are, at most, minimal ( $\lesssim 0.1$  dex). We find that the  $[\text{Cu}/\text{H}]$  ratios derived from Cu II lines are  $0.36 \pm 0.06$  dex larger than those derived from Cu I lines in the most metal-poor stars ( $[\text{Fe}/\text{H}] < -1.8$ ), suggesting that LTE underestimates the Cu abundance derived from Cu I lines. The deviations decrease in more metal-rich stars. Our results validate previous theoretical non-LTE calculations for both Cu and Zn, supporting earlier conclusions that the enhancement of  $[\text{Zn}/\text{Fe}]$  in metal-poor stars is legitimate, and the deficiency of  $[\text{Cu}/\text{Fe}]$  in metal-poor stars may not be as large as previously thought.

*Keywords:* nuclear reactions, nucleosynthesis, abundances — stars: abundances — stars: atmospheres — stars: individual (HD 19445, HD 76932, HD 84937, HD 94028, HD 140283, HD 160617) — stars: population II — ultraviolet: stars

## 1. INTRODUCTION

One key objective in the study of late-type stellar abundances is to identify the limits of calculations made assuming that local thermodynamic equilibrium (LTE) holds in the line-forming layers of the atmosphere. Of

particular interest are the elements copper (Cu,  $Z = 29$ ) and zinc (Zn,  $Z = 30$ ), two of the heaviest Fe-group elements. The  $[\text{Cu}/\text{Fe}]$  and  $[\text{Zn}/\text{Fe}]$  ratios deviate significantly from their Solar ratios in the most metal-poor stars, which have presumably been enriched by metals from limited numbers of earlier nucleosynthesis events. Specifically,  $[\text{Cu}/\text{Fe}]$  is substantially sub-Solar in stars with  $[\text{Fe}/\text{H}] \lesssim -2$ , exhibiting a plateau around  $[\text{Cu}/\text{Fe}] \approx -0.7$  to  $-1.0$  or a very slight decrease in  $[\text{Cu}/\text{Fe}]$  with decreasing  $[\text{Fe}/\text{H}]$  (e.g., Sneden et al. 1991; Mishenina et al. 2002; Bihain et al. 2004; Cayrel et al. 2004; Lai et al. 2008; Sobeck et al. 2008; Ishigaki et al. 2013). The  $[\text{Zn}/\text{Fe}]$  ratio increases to super-Solar ratios as  $[\text{Fe}/\text{H}]$  decreases (e.g., in addition to many of the studies listed above, Barklem et al. 2005; Nissen et al. 2007; Saito et al. 2009; Roederer et al. 2010; Hollek et al. 2011; Cohen et al. 2013; Jacobson et al. 2015; Reggiani et al. 2017). It is important that these trends are characterized reliably so that models of supernova nucleosynthesis and chemical evolution can be tuned appropriately (e.g., Timmes et al. 1995; Goswami & Prantzos 2000; François et al. 2004; Kobayashi et al. 2006; Ro-

Email: iur@umich.edu

\* Based on observations made with the NASA/ESA *Hubble Space Telescope*, obtained from the data archive at the Space Telescope Science Institute (STScI), which is operated by the Association of Universities for Research in Astronomy, Inc. (AURA) under NASA contract NAS 5-26555. This work is supported by NASA through grant number AR-15051 and makes use of data from programs GO-7348, GO-8197, GO-9804, GO-14161, and GO-14672. This research has also made use of the Keck Observatory Archive (KOA), which is operated by the W.M. Keck Observatory and the NASA Exoplanet Science Institute (NExScI), under contract with NASA. These data are associated with programs C314Hr, H6aH, and H283Hr. Other data has been obtained from the European Southern Observatory (ESO) Science Archive Facility. These data are associated with programs 65.L-0507(A), 67.D-0439(A), and 080.D-0347(A). This work has also made use of data collected from McDonald Observatory of the University of Texas at Austin.

mano & Matteucci 2007; Hirai et al. 2018). The  $[\text{Zn}/\text{H}]$  ratios in Galactic stars also serve as a metallicity reference to compare with damped Lyman- $\alpha$  systems, where Zn remains largely in the gas phase (e.g., Pettini et al. 1994; Prochaska & Wolfe 1999; Akerman et al. 2005; Rafelski et al. 2012).

These stellar abundances are based on LTE radiative transfer calculations in standard one-dimensional, hydrostatic model atmospheres. Takeda et al. (2005) performed the first non-LTE calculations of three optical Zn I lines (at 4722, 4810, and 6362 Å) to reassess  $[\text{Zn}/\text{Fe}]$  ratios in metal-poor stars with  $-4 < [\text{Fe}/\text{H}] < 0$ . They found minor non-LTE corrections to the LTE abundances, usually  $< 0.1$  dex, in the sense that LTE underestimates the abundance. The corrections were largest in the most metal-poor stars, mildly exaggerating the observed  $[\text{Zn}/\text{Fe}]$  enhancement in low-metallicity stars.

Yan et al. (2015) used the Cu model atom developed by Shi et al. (2014) to perform non-LTE calculations for three high-excitation optical Cu I lines (at 5105, 5218, and 5782 Å) in late-type stars with  $-1.6 < [\text{Fe}/\text{H}] < -0.1$ . Each of these lines behaved slightly differently when calculated in non-LTE, but all showed significant positive corrections to the LTE abundances. The corrections were smallest for the metal-rich stars,  $\approx +0.03$  dex, and increased to nearly  $\approx +0.20$  dex for the most metal-poor star. Yan et al. (2016) obtained similar results when they applied non-LTE calculations to rederive  $[\text{Cu}/\text{Fe}]$  ratios in the sample of Nissen & Schuster (2010). Andrievsky et al. (2018) performed non-LTE calculations for Cu I lines in dwarf and giant stars spanning  $-4.2 < [\text{Fe}/\text{H}] < -1.4$ . For the lowest-metallicity stars in their sample, which were cool giants, only the Cu I resonance lines at 3247 and 3273 Å were available. The non-LTE corrections were substantially larger in these cases, ranging from  $\approx +0.5$  to  $+1.2$  dex in seven stars with  $[\text{Fe}/\text{H}] < -2$ . That study was also able to resolve the issue of discrepant abundances derived from the Cu I lines at 3273 and 5105 Å, an effect noticed in a metal-poor giant star by Bonifacio et al. (2010). Yan et al. and Andrievsky et al. had one line (Cu I  $\lambda 5105$  Å) in one star (HD 94028) in common, and they derived different non-LTE corrections to the Cu abundance,  $+0.17$  dex and  $+0.48$  dex, respectively. Andrievsky et al. attributed this discrepancy to differences in the adopted model atoms.

One way to test the reliability of the non-LTE calculations for Cu and Zn is to derive abundances from Cu II and Zn II lines, which arise from the majority species of each atom and should be relatively immune to non-LTE effects. The challenge is that Cu II and Zn II lines are only found in the ultraviolet (UV) part of the spectrum of late-type stars, far below the atmospheric cutoff. Acquiring such spectra requires access to an echelle spectrograph in space. Roederer & Lawler (2012) made the first such attempts, using a high-resolution ( $R \equiv \lambda/\Delta\lambda \sim 114,000$ ) UV spectrum of

the metal-poor subgiant star HD 160617. One UV Zn II line gave concordant results with several optical Zn I lines, but the UV Cu II lines predicted abundances about a factor of two higher than the optical Cu I lines. Roederer et al. (2014b) conducted a study of high-resolution (but less so,  $R \sim 30,000$ ) UV spectra of two metal-poor giants, finding similar results, but with large ( $\approx 0.3$ – $0.5$  dex) uncertainties that could mask substantial differences. Roederer et al. (2016a) also studied Cu I and II and Zn I and II lines in the metal-poor main sequence star HD 94028, reporting agreement between the neutral and ionized species, but with combined uncertainties  $\approx 0.20$ – $0.25$  dex. Andrievsky et al. (2018) analyzed high-resolution UV spectra of two warm, metal-poor stars, finding that their Cu II lines yielded LTE abundances consistent with non-LTE calculations for optical Cu I lines. For completeness, we note that Zn can only be detected via resonance lines of Zn I and Zn II in the UV in the most metal-poor stars (Roederer et al. 2016b).

Here, we present a fresh reanalysis of Cu I and II and Zn I and Zn II lines in six stars with high-quality UV spectra. We minimize systematic effects by (1) selecting stars with a limited range of effective temperatures ( $T_{\text{eff}}$ ) and surface gravities ( $\log g$ ); (2) rederiving stellar parameters and metallicities by a consistent method; and (3) analyzing the lines in a consistent manner with the same atomic line data, grid of model atmospheres, and line analysis code. This enables us to assess the reliability of LTE calculations for Cu I and Zn I lines in warm, metal-poor stars and check the reliability of the non-LTE calculations.

Throughout this work, we adopt the standard nomenclature for elemental abundances and ratios. For element X, the absolute abundance is defined as the number of X atoms per  $10^{12}$  H atoms,  $\log \epsilon(X) \equiv \log_{10}(N_X/N_H) + 12.0$ . For elements X and Y, the abundance ratio relative to the Solar ratio is defined as  $[\text{X}/\text{Y}] \equiv \log_{10}(N_X/N_Y) - \log_{10}(N_X/N_Y)_\odot$ . We adopt the Solar photospheric abundances of Asplund et al. (2009):  $\log \epsilon(\text{Fe}) = 7.50$ ,  $\log \epsilon(\text{Cu}) = 4.19$ , and  $\log \epsilon(\text{Zn}) = 4.56$ . By convention, abundances or ratios denoted with the ionization state are understood to be the total elemental abundance as derived from transitions of that particular ionization state after Saha ionization corrections have been applied.

## 2. OBSERVATIONS

We download UV spectra from the Mikulski Archive for Space Telescopes (MAST). These spectra were collected using the Space Telescope Imaging Spectrograph (STIS; Kimble et al. 1998; Woodgate et al. 1998) on board the *Hubble Space Telescope* (HST). We consider a star for inclusion in the sample if extant  $R \sim 30,000$  or  $R \sim 114,000$  spectra cover at least  $2037 \leq \lambda \leq 2127$  Å, where the Cu II and Zn II lines are found. Inspection of the data reveals that stars that are warm ( $T_{\text{eff}} > 5600$  K) and metal-poor ( $[\text{Fe}/\text{H}] < -1.0$  or so) with  $R \sim 114,000$

spectra provide tolerable levels of line blending and a reliable estimate of the local continuum. The STIS  $R \sim 114,000$  observations were made using the E230H echelle grating, the  $0''.09 \times 0''.2$  slit, and the NUV Multi-anode Microchannel Array detector. The six stars meeting these criteria are listed in Table 1 along with the instrument, program identification (ID) number, datasets, principle investigator (PI), resolving power, and signal-to-noise (S/N) ratio per pixel in the continuum at a reference wavelength.

We supplement the UV spectra with high-resolution optical spectra downloaded from online archives, including the European Southern Observatory (ESO) Science Archive Facility and the Keck Observatory Archives (KOA). These data were collected with the Ultraviolet and Visual Echelle Spectrograph (UVES; Dekker et al. 2000) on the Very Large Telescope, the High Accuracy Radial velocity Planet Searcher (HARPS; Mayor et al. 2003) on the ESO 3.6 m Telescope at La Silla, and the High Resolution Echelle Spectrometer (HIRES; Vogt et al. 1994) on the Keck I Telescope. Table 1 lists the instrument, program ID number, PI, resolving power, and S/N ratio associated with these data. An optical spectrum of one star was collected previously using the Robert G. Tull Coudé Spectrograph (Tull et al. 1995) at the Harlan J. Smith Telescope at McDonald Observatory (see details in Roederer et al. 2014a). The McDonald Observatory does not have an online archive, and this spectrum may be obtained by contacting IUR directly.

### 3. STELLAR PARAMETERS

#### 3.1. Fe Lines

We compile a list of Fe I lines with reliable oscillator strengths from the National Institute of Standards and Technology (NIST) Atomic Spectral Database (ASD; Kramida et al. 2017b) with grades C or better ( $\leq 25\%$  uncertainty, or 0.12 dex). These  $\log gf$  values mainly come from work by O’Brian et al. (1991). We supplement this list with results from recent laboratory studies by Den Hartog et al. (2014) and Ruffoni et al. (2014), whose uncertainties are generally reliable to better than 5% (0.02 dex). We discard any Fe I lines with lower excitation potential (E.P.) levels less than 1.2 eV, because previous studies have shown that these lines may yield higher-than-average abundances in metal-poor dwarfs and giants (e.g., Cayrel et al. 2004; Cohen et al. 2008, 2013; Lai et al. 2008; Bergemann et al. 2012).

We adopt  $\log gf$  values for Fe II lines from Meléndez & Barbuy (2009). Their values for the Fe II lines in our study were obtained by renormalizing relative theoretical  $\log gf$  values within a given multiplet to an absolute scale set by laboratory measurements of the upper level lifetime. We also discuss consideration of an alternative set of Fe II  $\log gf$  values from NIST, with  $\log gf$  grades C or better, in Section 3.2.

We measure equivalent widths (EWs) of Fe lines using a semi-automatic routine that fits Voigt or Gaussian line profiles to continuum-normalized spectra (Roederer et al. 2014a). We visually inspect each line, and any line determined to be blended, suffer from uncertain continuum placement, or otherwise compromised is discarded from consideration. We retain 97–152 Fe I lines and 12–17 Fe II lines, spanning 3724–7749 Å, and these lines and our EW measurements are reported in Table 2.

#### 3.2. Model Atmosphere Parameters

All stars in the sample are relatively bright and nearby, so broadband photometry is readily available. Optical and near-infrared magnitudes for these stars are available in catalogs by Ducati (2002) and Munari et al. (2014) for Johnson  $B$  and  $V$ , the Two Micron All Sky Survey (2MASS; Cutri et al. 2003) for  $J$ ,  $H$ , and  $K$ ; and Paunzen (2015) for Strömgren-Crawford  $b$  and  $y$ . We construct six colors with calibrated color- $T_{\text{eff}}$  relations ( $B - V$ ,  $V - J$ ,  $V - H$ ,  $V - K$ ,  $J - K$ , and  $b - y$ ). We adopt reddening estimates from Casagrande et al. (2011). These stars are located in the foreground of the reddening layer, so  $E(B - V) < 0.005$  for all six stars (see also Meléndez et al. 2010). We deredden colors according to the extinction coefficients of McCall (2004).

Parallaxes calculated from the *Tycho-2 Gaia* Astrometric Solution (*Gaia* Data Release 1; Gaia Collaboration et al. 2016) are available for 5 stars in the sample. A parallax measurement for the other star (HD 84937) is available from the *Hipparcos* re-reduction by van Leeuwen (2007). For the other five stars, the *Hipparcos* and *Tycho-2/Gaia* parallaxes agree to better than their  $1.6\sigma$  combined uncertainties.

We adopt  $T_{\text{eff}}$  values calculated from the Casagrande et al. (2010) metallicity-dependent color- $T_{\text{eff}}$  calibrations. For each star, the final  $T_{\text{eff}}$  is determined using a Monte Carlo resampling method. We draw  $10^4$  samples from each input parameter (magnitudes, reddening, and metallicity). We assume Gaussian uncertainties, including conservative minimum uncertainties of 0.02 mag in magnitude, 0.02 mag in  $E(B - V)$ , and 0.3 dex in metallicity. Each calculation is self-consistent and uses the same set of input draws, and we adopt the median of the final distribution as  $T_{\text{eff}}$ . We estimate the uncertainty as the quadrature sum of the standard deviation of the Casagrande et al.  $T_{\text{eff}}$  distribution and the standard deviation of the  $T_{\text{eff}}$  values predicted by the Casagrande et al., Alonso et al. (1999), and Ramírez & Meléndez (2005) color- $T_{\text{eff}}$  calibrations. We report these values in Table 3.

We calculate  $\log g$  from fundamental relations:

$$\log g = 4 \log T_{\text{eff}} + \log(M/M_{\odot}) - 10.61 + 0.4(BC_V + V - 5 \log d + 5 - 3.1E(B - V) - M_{\text{bol},\odot}). \quad (1)$$

Here,  $M$  is the mass of the star (Casagrande et al. 2010),  $BC_V$  is the bolometric correction in the  $V$  band

**Table 1.** Characteristics of Archival UV and Optical Spectra

| Star            | Instrument | Program ID    | Datasets                   | PI         | $R$                         | S/N <sup>a</sup> |
|-----------------|------------|---------------|----------------------------|------------|-----------------------------|------------------|
| UV Spectra      |            |               |                            |            |                             |                  |
| HD 19445        | STIS       | GO-14672      | OD65A1010-A8030            | Peterson   | 114,000                     | 50               |
| HD 76932        | STIS       | GO-9804       | O8P201010-02040            | Duncan     | 114,000                     | 55               |
| HD 84937        | STIS       | GO-14161      | OCTKA0010-AD030            | Peterson   | 114,000                     | 45               |
| HD 94028        | STIS       | GO-8197       | O5CN01010-03040            | Duncan     | 114,000                     | 65               |
| HD 140283       | STIS       | GO-7348       | O55Z01030-01050, O55Z02010 | Edvardsson | 114,000                     | 45               |
| HD 160617       | STIS       | GO-8197       | O5CN04010-54050            | Duncan     | 114,000                     | 25               |
| Optical Spectra |            |               |                            |            |                             |                  |
| HD 19445        | HIRES      | H283Hr        | ...                        | Boesgaard  | 49,000                      | 550              |
| HD 76932        | UVES       | 67.D-0439(A)  | ...                        | Primas     | 49,600; 57,000 <sup>b</sup> | 310              |
| HD 84937        | HIRES      | C314Hr        | ...                        | Gal-Yam    | 49,000                      | 190              |
| HD 94028        | Tull       | <sup>c</sup>  | ...                        | Roederer   | 30,000                      | 140              |
| HD 140283       | UVES       | 67.D-0439(A)  | ...                        | Primas     | 49,600                      | ...              |
|                 | HARPS      | 080.D-0347(A) | ...                        | Heiter     | 115,000                     | 230              |
| HD 160617       | UVES       | 65.L-0507(A)  | ...                        | Primas     | 49,600                      | ...              |
|                 | HIRES      | H6aH          | ...                        | Boesgaard  | 49,000                      | 160              |

<sup>a</sup> S/N values are given at 2100 Å and 5000 Å for the UV and optical spectra, respectively

<sup>b</sup> Values for the blue and red components of the spectrum

<sup>c</sup> See Roederer et al. (2014a) for observational details

**Table 2.** Fe Lines and EWs

| Star    | Species | $\lambda$ | E.P. | $\log gf$ | EW   |
|---------|---------|-----------|------|-----------|------|
|         |         | (Å)       | (eV) |           | (mÅ) |
| HD19445 | FeI     | 4001.66   | 2.18 | -1.90     | 12.1 |
| HD19445 | FeI     | 4005.24   | 1.56 | -0.61     | 87.9 |
| HD19445 | FeI     | 4009.71   | 2.22 | -1.25     | 31.0 |

NOTE—The complete version of Table 2 is available in the online edition of the journal. A sample is shown here to illustrate its form and content.

(Casagrande & Vandenberg 2014),  $V$  is the apparent magnitude, and  $d$  is the distance in pc, which is calculated from the parallax measurement.  $M_{\text{bol},\odot}$  is the Solar bolometric magnitude, 4.75, and the constant 10.61 is calculated from the Solar constants  $\log T_{\text{eff},\odot} = 3.7617$  and  $\log g_{\odot} = 4.438$ . We draw  $10^4$  samples from each of these input parameters. The median of these calculations gives the  $\log g$  value, and their standard deviation gives the uncertainty. We report these values in Table 3. The  $T_{\text{eff}}$  and  $\log g$  values for these stars place them on the main sequence or slightly evolved beyond the turnoff point.

We interpolate model atmospheres from the  $\alpha$ -enhanced ATLAS9 grid of models (Castelli & Kurucz 2003), using an interpolation code provided by A. McWilliam (2009, private communication). We derive Fe abundances using a recent version of the LTE line analysis software MOOG (Snedden 1973; 2017 version). Rayleigh scattering, which affects the continuous

opacity at shorter wavelengths, is treated as isotropic, coherent scattering as described in Sobek et al. (2011). We adopt damping constants for collisional broadening with neutral hydrogen from Barklem & O’Mara (2000) and Barklem & Aspelund-Johansson (2005), when available, otherwise we adopt the standard Unsöld (1955) recipe, except as noted in Section 4.1.

We iteratively determine the microturbulent velocity,  $v_t$ , and model metallicity,  $[M/H]$ . Lines yielding an abundance more than 0.4 dex from the mean are culled. Convergence is reached when there is no dependence between line strength and abundance derived from Fe I lines, and when the input  $[M/H]$  agrees with the derived  $[Fe/H]$  ratios to within 0.1 dex. Metallicity uncertainties are estimated by drawing 250 samples of model parameters and EWs from normal distributions, assuming a 5% uncertainty in each EW measurement. We recompute the abundance for each set, and the standard deviation of the results is adopted as the uncertainty. These values are also listed in Table 3.

The agreement between Fe abundances derived from Fe I and Fe II lines is superb. The mean difference, in the sense of  $[Fe\ II/H] - [Fe\ I/H]$ , is  $+0.02 \pm 0.02$  ( $\sigma = 0.05$ ). Our method of deriving model parameters and Fe abundances does not enforce Boltzmann excitation equilibrium or Saha ionization equilibrium, so this agreement does not result by construction. Instead, when Fe I lines with E.P.  $< 1.2$  eV are excluded, departures from LTE in neutral Fe are relatively small for the stars in this sample. This matches predictions from non-LTE calculations, which show that most Fe II lines are essentially in LTE and the amount of Fe I over-ionization has a mi-

**Table 3.** *V* Magnitudes, Model Atmosphere Parameters, and Derived Iron Abundances

| Star      | <i>V</i> | $T_{\text{eff}}$ | $\log g$    | $v_t$                 | [M/H]      | [Fe I/H]     | [Fe II/H]    | [Fe II/H]−[Fe I/H] |
|-----------|----------|------------------|-------------|-----------------------|------------|--------------|--------------|--------------------|
|           | (mag)    | (K)              | [cgs]       | (km s <sup>−1</sup> ) |            |              |              |                    |
| HD 19445  | 8.06     | 6070 ± 76        | 4.44 ± 0.14 | 1.60 ± 0.10           | −2.2 ± 0.1 | −2.12 ± 0.05 | −2.15 ± 0.04 | −0.03 ± 0.07       |
| HD 76932  | 5.86     | 5945 ± 93        | 4.17 ± 0.11 | 1.10 ± 0.10           | −1.0 ± 0.1 | −0.95 ± 0.07 | −0.95 ± 0.06 | +0.00 ± 0.10       |
| HD 84937  | 8.32     | 6427 ± 93        | 4.14 ± 0.14 | 1.45 ± 0.10           | −2.2 ± 0.1 | −2.16 ± 0.06 | −2.11 ± 0.05 | +0.05 ± 0.07       |
| HD 94028  | 8.22     | 6097 ± 74        | 4.34 ± 0.14 | 1.30 ± 0.10           | −1.6 ± 0.1 | −1.52 ± 0.05 | −1.53 ± 0.05 | −0.01 ± 0.07       |
| HD 140283 | 7.22     | 5766 ± 64        | 3.64 ± 0.13 | 1.30 ± 0.10           | −2.6 ± 0.1 | −2.59 ± 0.05 | −2.50 ± 0.05 | +0.09 ± 0.06       |
| HD 160617 | 8.74     | 6050 ± 67        | 3.91 ± 0.13 | 1.50 ± 0.10           | −1.9 ± 0.1 | −1.89 ± 0.04 | −1.84 ± 0.04 | +0.05 ± 0.06       |

nor impact ( $\lesssim 0.1$  dex) in warm, metal-poor stars (e.g., Mashonkina et al. 2011; Bergemann et al. 2012; Sitnova et al. 2015).

However, the choice of which  $\log gf$  scale to adopt for Fe II lines plays a significant role in determining the level of agreement. The NIST  $\log gf$  values for Fe II decrease the [Fe II/H] ratios by 0.09–0.15 dex, and the average [Fe II/H]−[Fe I/H] would be  $-0.10 \pm 0.03$  ( $\sigma = 0.07$ ). The NIST  $\log gf$  values for the Fe II lines in our study have typical uncertainties of 0.12 dex, so the differences between the NIST and Meléndez & Barbuy (2009)  $\log gf$  scales are within the stated uncertainties. We trust that future laboratory work may help to improve these values. In the meantime, we note that the key results of the present study, the [Cu II/Cu I] and [Zn II/Zn I] ratios, are calculated independently from the [Fe/H] ratios.

### 3.3. Comparison with Previous Results

We now compare our  $T_{\text{eff}}$ ,  $\log g$ , and [Fe/H] values with those from previous work. We select studies for comparison that have at least three stars in common with our sample. We also require that the previous study derived at least one of the ratios [Cu/Fe] or [Zn/Fe] for each star, which we use for further comparisons in Section 4.3. Six studies meet these criteria: Sneden et al. (1991), Mishenina & Kovtyukh (2001) and Mishenina et al. (2002) (considered as one), Bihain et al. (2004), Nissen et al. (2007), Roederer (2012), and Bensby et al. (2014).

For HD 19445, HD 76932, HD 84937, HD 94028, HD 140283, and HD 160617, this results in a total number of stellar parameter comparisons of 3, 5, 5, 4, 6, and 2 stars, respectively. We find no evidence that our values differ substantially from previous work. The differences between our  $T_{\text{eff}}$ ,  $\log g$ , and [Fe/H] values all agree to better than 2 standard deviations of the mean of those from previous studies for all stars except HD 160617. Only two previous studies meet our criteria for HD 160617, Nissen et al. (2007) and Bensby et al. (2014). Our  $T_{\text{eff}}$  value is in good agreement with previous work. The  $\log g$  and [Fe/H] values of the two previous studies agree to within a few hundredths of a dex, producing small standard deviations. Our  $\log g$  value is higher than their mean by only 0.06 dex, and our [Fe/H]

**Table 4.** Atomic Data for Cu and Zn Lines

| Species | $\lambda$ | E.P. | $\log gf$ |
|---------|-----------|------|-----------|
|         | (Å)       | (eV) |           |
| Cu I    | 3247.54   | 0.00 | −0.05     |
|         | 3273.96   | 0.00 | −0.35     |
|         | 5105.54   | 1.39 | −1.50     |
| Cu II   | 5218.20   | 3.82 | +0.26     |
|         | 2037.13   | 2.83 | −0.23     |
|         | 2054.98   | 2.83 | −0.29     |
|         | 2104.80   | 2.98 | −0.51     |
| Zn I    | 2126.04   | 2.83 | −0.23     |
|         | 2138.56   | 0.00 | +0.16     |
|         | 3075.90   | 0.00 | −3.85     |
|         | 3302.58   | 4.03 | −0.02     |
|         | 4680.14   | 4.01 | −0.85     |
| Zn II   | 4722.15   | 4.03 | −0.37     |
|         | 4810.53   | 4.08 | −0.15     |
|         | 2062.00   | 0.00 | −0.29     |

value is lower than their mean by only 0.12 dex. Both of these are well within the combined uncertainties, and we regard the stellar parameters of HD 160617 as also being in agreement with previous work.

## 4. COPPER AND ZINC ABUNDANCE ANALYSIS

### 4.1. Cu and Zn Lines

Several Cu I and Zn I lines are found in the optical part of the spectrum, while the Cu II and Zn II lines are only found in the UV. Table 4 lists the wavelengths, E.P., and  $\log gf$  values for the lines used in this study.

We adopt the  $\log gf$  values for the Cu I lines at 3247.54 and 3273.96 Å from NIST. Both values have grades of AA, indicating uncertainties  $\leq 1\%$  (0.004 dex). The  $\log gf$  values of the Cu I lines at 5105.54 and 5218.20 Å each have C+ grades ( $< 18\%$ , 0.09 dex), according to NIST. Additional Cu I lines at 5700.24 and 5782.13 Å are not reliably detected in our spectra.

Roederer & Lawler (2012) evaluated the quality of oscillator strengths available for seven Cu II lines. Kramida et al. (2017a) have released an updated critical compilation of Cu II oscillator strengths, which are in-

cluded in the most recent NIST ASD update. The two sets of oscillator strengths agree to within their stated uncertainties, and we simply adopt the values recommended by Roederer & Lawler. Four of these lines, listed in Table 4, are detected in most of our spectra.

Roederer & Lawler (2012) also evaluated the oscillator strengths for Zn I lines commonly used in abundance analyses of late-type stars, and we adopt those recommended values. Their uncertainties range from 0.02 to 0.08 dex. We adopt the  $\log gf$  value for the Zn I line at 2138.56 Å from NIST.

We adopt the  $\log gf$  value for the Zn II resonance line at 2062.00 Å from the work of Bergeson & Lawler (1993), who estimated an uncertainty of 0.03 dex. The other Zn II resonance line at 2025.48 Å is too blended to be useful as an abundance indicator.

The Zn II resonance line ( $4s^2S - 4p^2P^o$ ) at 2062.00 Å is saturated in all stars in the sample, and its abundance sensitivity is expressed through its damping wings. We calculate the broadening of this line with neutral hydrogen atoms using the Anstee, Barklem and O’Mara (ABO) theory, originally developed for neutral species (e.g., Anstee & O’Mara 1991, 1995; Barklem & O’Mara 1997), and extended to singly-ionized species by Barklem & O’Mara (1998). The neutral and singly-ionized cases differ in that an approximation originally due to Unsöld (1955) is not expected to be generally valid for ions. Specifically, an energy debt parameter,  $E_p$ , appearing in the ABO theory is approximated to  $E_p = -4/9$  atomic units for neutrals, but for ions it is usually calculated in detail on a line-by-line basis. However, such calculations require good knowledge of the fundamental atomic data (wavelengths, oscillator strengths) for transitions in the ion. Lack of such data for Zn II means that a detailed calculation of  $E_p$  is not possible. Thus, we calculate the broadening with the Unsöld approximation value,  $E_p = -4/9$  atomic units. Within this approximation we obtain the broadening cross section at relative velocity  $v = 10^4$  m/s to be 161 atomic units, with a velocity dependence parameter  $\alpha = 0.30$  (see Anstee & O’Mara 1995). The log of the line width (full width at half maximum) per perturber at  $10^4$  K is  $-7.9394$  rad s $^{-1}$  cm $^3$ . Test calculations reveal that the resonance line is not terribly sensitive to this assumption. Doubling or halving the value of  $E_p$ , which roughly spans the range of values seen in other atoms (Barklem & O’Mara 1998, 2000; Barklem & Aspelund-Johansson 2005), leads to variation of the cross section by at most 25%, and this is perhaps indicative of the error in the calculated value. We note that for Fe II,  $E_p = -4/9$  atomic units is in fact a good approximation for the vast majority of levels (see Figure 2 of Barklem & Aspelund-Johansson 2005).

Cu is an odd- $Z$  element with two  $I = 3/2$  isotopes,  $^{63}\text{Cu}$  and  $^{65}\text{Cu}$ , giving rise to hyperfine structure (HFS) and isotope shifts (IS) that may impact the observed line profiles and derived abundances. We adopt a So-

lar isotope mixture for Cu in our syntheses. For Cu I, we adopt the HFS/IS patterns given by the Kurucz (2011) database. No modern measurements of the IS, magnetic dipole, or electric quadrupole are available for the levels connected by our Cu II transitions of interest. Roederer & Lawler (2012) assembled trial HFS/IS patterns from early work by Elbel et al. (1963) and Elbel & Hühnermann (1969) for the Cu II line at 2126 Å to gauge the potential impact of neglecting the HFS/IS on the derived abundances, and we repeat this exercise here. For most stars, there is no discernible impact at the 0.01 dex level. Only in the most metal-rich stars, HD 76932 and HD 94028, do the HFS/IS component patterns result in a mild abundance decrease, by 0.04 and 0.02 dex, respectively. Data are not available for the other Cu II lines of interest here. We conclude that the derived Cu II abundances in HD 76932 and HD 94028 could be overestimated by a few hundredths of a dex. No HFS/IS component patterns are considered for any Zn I or II line.

#### 4.2. Abundances

We derive abundances for all Cu and Zn lines by comparing the observed line profiles to MOOG synthetic spectra with varied Cu or Zn abundances. We generate line lists using a modified version of the *linemake* code (C. Sneden 2017, private communication), which includes additional updates for UV transitions relevant to late-type stellar spectra. This code replaces the Kurucz (2011) line list entries with wavelengths,  $\log gf$  values, molecular lines, and HFS/IS component patterns from modern experimental work. Lawler et al. (2009, 2017) summarize the methods and limitations of these laboratory efforts.

Abundances derived from individual Cu I and II lines are reported in Table 5, and abundances derived from individual Zn I and II lines are reported in Table 6. Table 7 lists the mean Cu abundance ratios, and Table 8 lists the mean Zn abundance ratios. The statistical uncertainty estimates account for the impact of noise, uncertainties in the continuum placement, minor blends, and  $\log gf$  values. The systematic uncertainty estimates account for the impact of uncertainties in the model atmosphere parameters. We estimate the systematic uncertainties by recomputing the Cu or Zn abundances in a series of 250 trials, each with a different set of approximate Cu or Zn EWs and model atmosphere parameters.

Figures 1 and 2 show the Cu and Zn lines used in HD 84937. We do not use the Cu I lines at 3247 and 3273 Å when they saturate in cooler and more metal-rich stars. We derive abundances from one or more Cu I resonance lines and one or more high-excitation lines in only two stars, but in these two cases we find no significant abundance discrepancies. Commentary on individual lines in the UV spectrum of HD 160617 may be found in Section 5 of Roederer & Lawler (2012). One Zn I line used in the present study, at 2138.56 Å, was

**Table 5.** Derived  $\log \epsilon$  Abundances and Uncertainties for Individual Cu Lines

| Star      | Cu I        |             |             |             | Cu II       |             |             |             |
|-----------|-------------|-------------|-------------|-------------|-------------|-------------|-------------|-------------|
|           | 3247.54 Å   | 3273.96 Å   | 5105.54 Å   | 5218.20 Å   | 2037.13 Å   | 2054.98 Å   | 2104.80 Å   | 2126.04 Å   |
| HD 19445  | 1.17 ± 0.10 | 1.25 ± 0.10 | ...         | ...         | 1.51 ± 0.10 | 1.55 ± 0.15 | 1.59 ± 0.15 | 1.57 ± 0.15 |
| HD 76932  | ...         | 3.07 ± 0.20 | 3.07 ± 0.05 | 3.15 ± 0.10 | 3.13 ± 0.20 | 3.07 ± 0.20 | 3.17 ± 0.20 | 3.19 ± 0.25 |
| HD 84937  | 1.15 ± 0.10 | 1.13 ± 0.05 | ...         | ...         | 1.37 ± 0.20 | 1.39 ± 0.10 | 1.57 ± 0.20 | 1.47 ± 0.10 |
| HD 94028  | 2.13 ± 0.25 | 2.09 ± 0.20 | 2.17 ± 0.20 | ...         | 2.27 ± 0.15 | 2.33 ± 0.15 | 2.45 ± 0.15 | 2.37 ± 0.15 |
| HD 140283 | 0.57 ± 0.10 | 0.61 ± 0.05 | ...         | ...         | ...         | 0.99 ± 0.20 | ...         | 0.97 ± 0.10 |
| HD 160617 | 1.31 ± 0.15 | 1.41 ± 0.10 | ...         | ...         | 1.75 ± 0.15 | 1.81 ± 0.15 | 1.92 ± 0.15 | 1.83 ± 0.15 |

NOTE—The stated uncertainties reflect the quality of the fit to the line profile, including factors like noise, blending features, and continuum placement.

**Table 6.** Derived  $\log \epsilon$  Abundances and Uncertainties for Individual Zn Lines

| Star      | Zn I        |             |             |             |             | Zn II       |             |
|-----------|-------------|-------------|-------------|-------------|-------------|-------------|-------------|
|           | 2138.56 Å   | 3075.90 Å   | 3302.58 Å   | 4680.14 Å   | 4722.15 Å   | 4810.53 Å   | 2062.00 Å   |
| HD 19445  | 2.68 ± 0.20 | 2.84 ± 0.25 | 2.58 ± 0.20 | 2.68 ± 0.15 | 2.64 ± 0.10 | 2.62 ± 0.05 | 2.68 ± 0.15 |
| HD 76932  | 3.80 ± 0.25 | ...         | 3.64 ± 0.20 | 3.80 ± 0.10 | 3.84 ± 0.05 | 3.84 ± 0.05 | 3.82 ± 0.10 |
| HD 84937  | ...         | 2.74 ± 0.20 | 2.82 ± 0.15 | ...         | 2.52 ± 0.10 | 2.56 ± 0.10 | 2.58 ± 0.15 |
| HD 94028  | 3.30 ± 0.20 | ...         | 3.22 ± 0.15 | 3.20 ± 0.10 | 3.20 ± 0.05 | 3.22 ± 0.05 | 3.34 ± 0.15 |
| HD 140283 | 2.18 ± 0.20 | 2.30 ± 0.15 | 2.14 ± 0.15 | 2.08 ± 0.20 | 2.24 ± 0.05 | 2.16 ± 0.05 | 2.30 ± 0.15 |
| HD 160617 | 2.99 ± 0.15 | 2.93 ± 0.10 | 2.82 ± 0.10 | 2.73 ± 0.20 | 2.82 ± 0.05 | 2.79 ± 0.05 | 2.94 ± 0.15 |

NOTE—The stated uncertainties reflect the quality of the fit to the line profile, including factors like noise, blending features, and continuum placement.

**Table 7.** Derived Cu Abundance Ratios

| Star      | [Cu I/H]            | [Cu I/Fe I]         | [Cu II/H]           | [Cu II/Fe II]       | [Cu II/H]−[Cu I/H]  |
|-----------|---------------------|---------------------|---------------------|---------------------|---------------------|
|           | ± stat. ± sys.      | ± stat. ± sys.      | ± stat. ± sys.      | ± stat. ± sys.      | ± stat. ± sys.      |
| HD 19445  | −2.98 ± 0.09 ± 0.11 | −0.86 ± 0.10 ± 0.12 | −2.65 ± 0.14 ± 0.05 | −0.50 ± 0.14 ± 0.06 | +0.33 ± 0.16 ± 0.12 |
| HD 76932  | −1.10 ± 0.23 ± 0.10 | −0.15 ± 0.24 ± 0.12 | −1.05 ± 0.19 ± 0.07 | −0.10 ± 0.20 ± 0.09 | +0.04 ± 0.29 ± 0.12 |
| HD 84937  | −3.06 ± 0.09 ± 0.10 | −0.88 ± 0.09 ± 0.12 | −2.75 ± 0.18 ± 0.05 | −0.64 ± 0.19 ± 0.07 | +0.31 ± 0.19 ± 0.11 |
| HD 94028  | −2.07 ± 0.16 ± 0.11 | −0.54 ± 0.17 ± 0.12 | −1.85 ± 0.16 ± 0.05 | −0.32 ± 0.17 ± 0.07 | +0.22 ± 0.23 ± 0.12 |
| HD 140283 | −3.59 ± 0.06 ± 0.09 | −1.00 ± 0.08 ± 0.10 | −3.21 ± 0.28 ± 0.05 | −0.71 ± 0.29 ± 0.07 | +0.38 ± 0.29 ± 0.10 |
| HD 160617 | −2.81 ± 0.10 ± 0.12 | −0.92 ± 0.11 ± 0.13 | −2.38 ± 0.16 ± 0.04 | −0.54 ± 0.17 ± 0.06 | +0.44 ± 0.19 ± 0.13 |

NOTE—The statistical uncertainties (“stat.”) include contributions from line fitting and  $\log gf$  values. The systematic uncertainties (“sys.”) include contributions from uncertainties in the model atmosphere parameters.

not discussed there. This line is blended with a Ni II line at 2138.58 Å. Fedchak & Lawler (1999) report an experimental  $\log gf$  for this Ni II line. The influence of this blending feature is minimal at low metallicity. Even in higher-metallicity stars, however, the high resolving power of the STIS E230H spectra enables us to derive abundances from the blue (short) side of the Zn I line that is largely unaffected by the blend with Ni II. This line yields abundances in good agreement with those de-

rived from Zn I lines in the optical spectrum, as can be inferred from Table 6.

### 4.3. Comparison with Previous Results

We now compare our derived [Cu/Fe] and [Zn/Fe] ratios with the previous studies listed in Section 3.3. For [Cu/Fe] in HD 19445, HD 76932, HD 84937, HD 94028, HD 140283, and HD 160617, this results in a total of 2, 3, 1, 2, 1, and 1 derivations in comparison stars. For [Zn/Fe], the same six stars have a total of 3, 5, 4, 4, 5, and 2 derivations in comparison stars. Our derived

**Table 8.** Derived Zn Abundance Ratios

| Star      | [Zn I/H]                  | [Zn I/Fe I]               | [Zn II/H]                 | [Zn II/Fe II]             | [Zn II/H]−[Zn I/H]        |
|-----------|---------------------------|---------------------------|---------------------------|---------------------------|---------------------------|
|           | ± stat. ± sys.            | ± stat. ± sys.            | ± stat. ± sys.            | ± stat. ± sys.            | ± stat. ± sys.            |
| HD 19445  | $-1.92 \pm 0.07 \pm 0.05$ | $+0.20 \pm 0.09 \pm 0.07$ | $-1.88 \pm 0.24 \pm 0.06$ | $+0.27 \pm 0.24 \pm 0.07$ | $+0.04 \pm 0.25 \pm 0.08$ |
| HD 76932  | $-0.73 \pm 0.06 \pm 0.06$ | $+0.22 \pm 0.09 \pm 0.09$ | $-0.74 \pm 0.20 \pm 0.07$ | $+0.21 \pm 0.20 \pm 0.09$ | $-0.01 \pm 0.21 \pm 0.09$ |
| HD 84937  | $-1.95 \pm 0.09 \pm 0.06$ | $+0.23 \pm 0.11 \pm 0.09$ | $-1.98 \pm 0.24 \pm 0.09$ | $+0.13 \pm 0.25 \pm 0.10$ | $-0.03 \pm 0.26 \pm 0.11$ |
| HD 94028  | $-1.35 \pm 0.06 \pm 0.04$ | $+0.18 \pm 0.08 \pm 0.06$ | $-1.22 \pm 0.24 \pm 0.06$ | $+0.31 \pm 0.25 \pm 0.08$ | $+0.13 \pm 0.25 \pm 0.07$ |
| HD 140283 | $-2.37 \pm 0.06 \pm 0.05$ | $+0.22 \pm 0.08 \pm 0.07$ | $-2.26 \pm 0.24 \pm 0.08$ | $+0.24 \pm 0.25 \pm 0.09$ | $+0.11 \pm 0.26 \pm 0.09$ |
| HD 160617 | $-1.74 \pm 0.06 \pm 0.05$ | $+0.15 \pm 0.07 \pm 0.06$ | $-1.62 \pm 0.24 \pm 0.07$ | $+0.22 \pm 0.24 \pm 0.08$ | $+0.12 \pm 0.25 \pm 0.09$ |

NOTE—The statistical uncertainties (“stat.”) include contributions from line fitting and  $\log gf$  values. The systematic uncertainties (“sys.”) include contributions from uncertainties in the model atmosphere parameters.

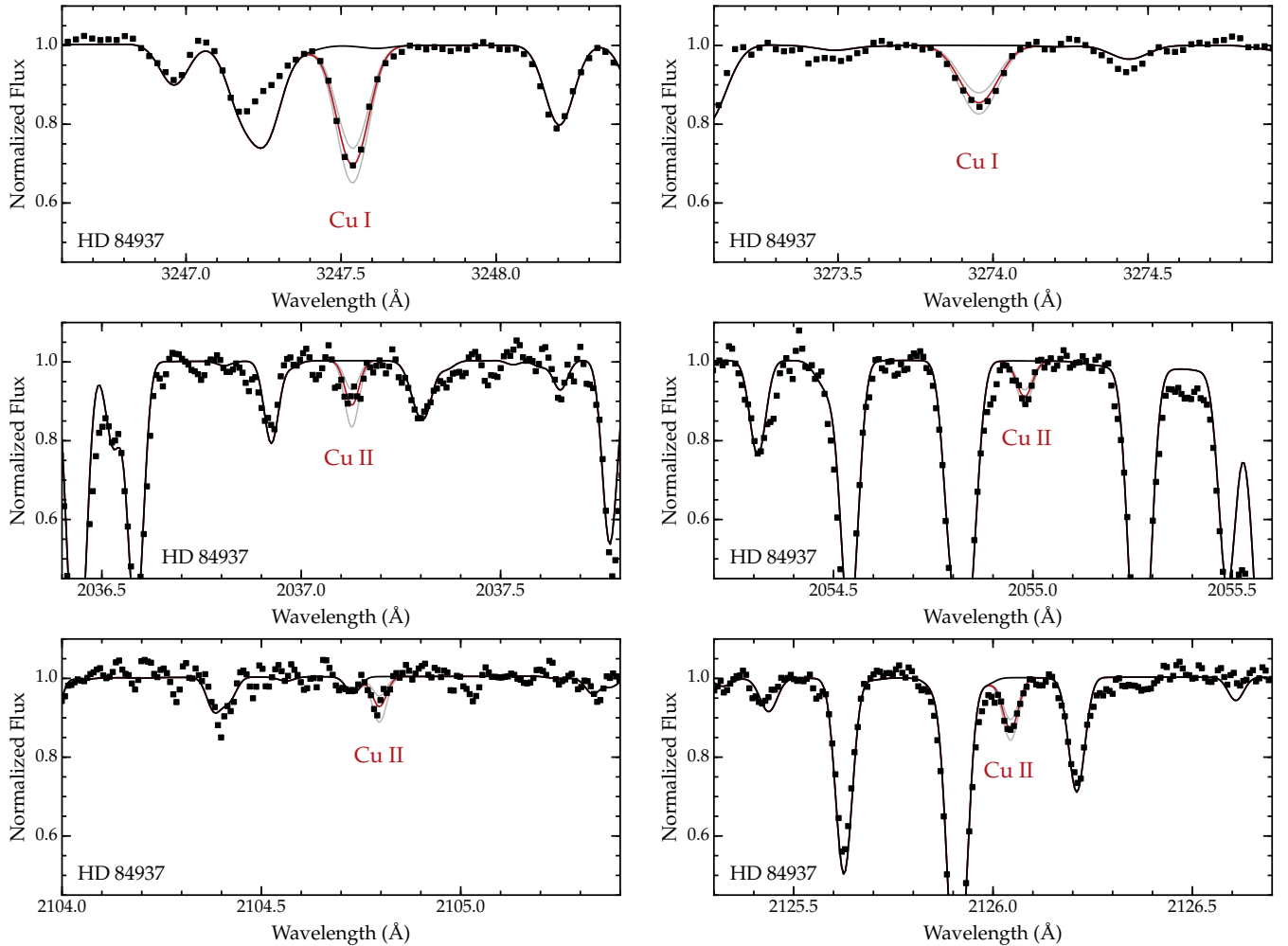


**Figure 1.** Comparison of observed and synthetic spectra for Cu I and II lines in HD 84937. The observed spectra are marked by filled squares. The red line marks the best-fit model spectrum, the gray lines mark the  $\pm 1\sigma$  uncertainties, and the black line marks a model spectrum with no Cu present.



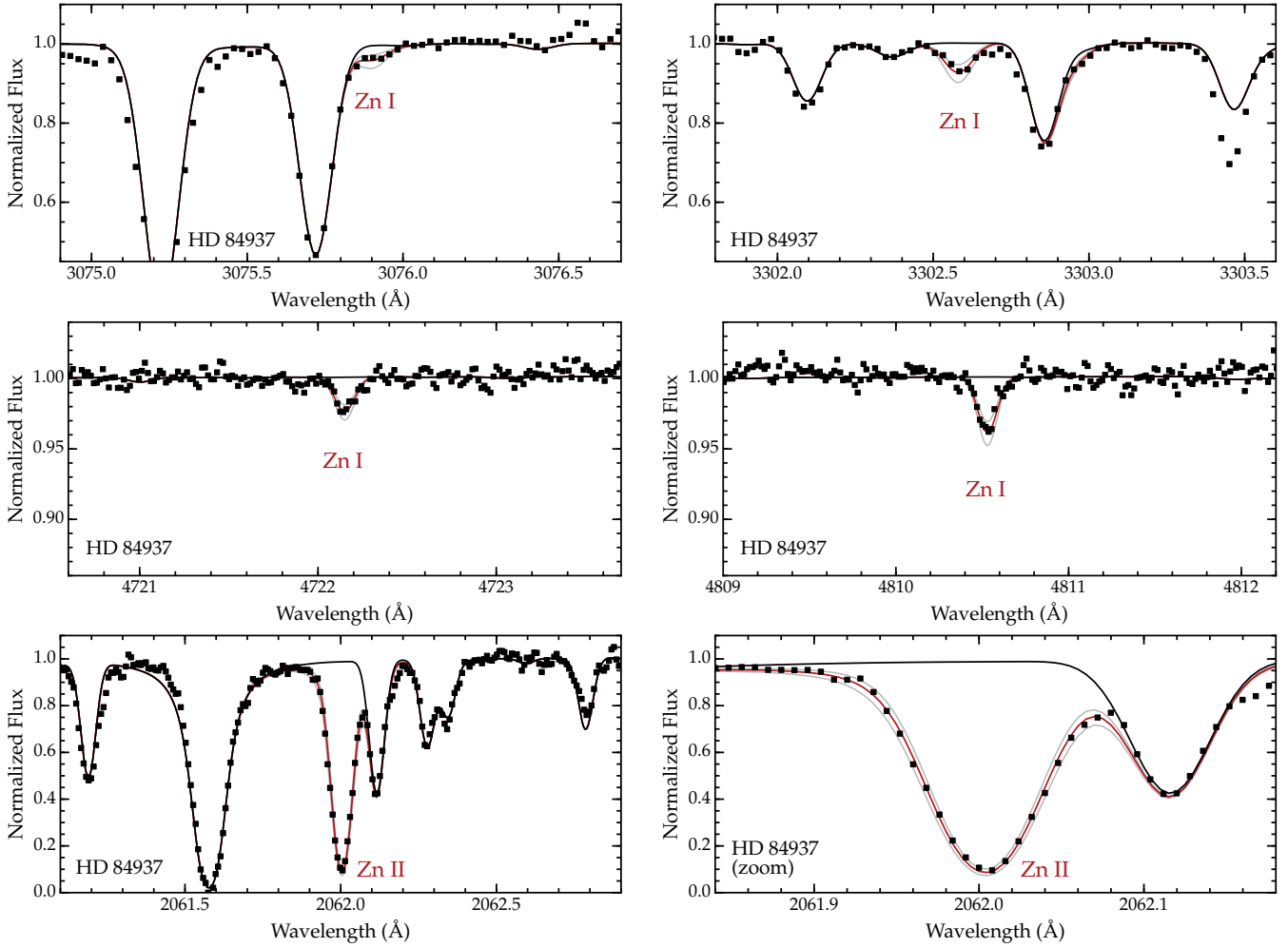


**Figure 2.** Comparison of observed and synthetic spectra for Zn I and II lines in HD 84937. The observed spectra are marked by filled squares. The red line marks the best-fit model spectrum, the gray lines mark the  $\pm 1\sigma$  uncertainties, and the black line marks a model spectrum with no Zn present. An additional Zn I line at 3302.94 Å is marginally discernible in the upper right panel. This line is too weak and blended to use as an abundance indicator. The lower right panel shows a zoom-in around the Zn II line at 2062.00 Å.

abundance ratios agree well in most cases, within 2 standard deviations of the mean of previous analyses.

One exception is [Cu/Fe] in HD 19445. We derive  $[\text{Cu}/\text{Fe}] = -0.86 \pm 0.16$  from Cu I lines, whereas Mishenina et al. (2002) derived  $-0.54 \pm 0.10$ . We use the two Cu I resonance lines in the blue part of the spectrum, while Mishenina et al. used three high-excitation Cu I lines in the red part of the spectrum. None of these high-excitation lines is visible in our HIRES spectrum. Mishenina et al. did not report the  $\log gf$  values adopted, so we cannot compare these with our own. The only other study that derived [Cu/Fe] in HD 19445, Bihain et al. (2004), found  $[\text{Cu}/\text{Fe}] = -0.65 \pm 0.14$  based on the resonance lines in the blue. Their result is consistent with both Mishenina et al. and us, so we do not regard this as a serious discrepancy.

The other exception, formally, is [Zn/Fe] in HD 84937. We derive  $[\text{Zn}/\text{Fe}] = +0.23 \pm 0.14$  from Zn I lines. Previously, Sneden et al. (1991) derived  $[\text{Zn}/\text{Fe}] = +0.14 \pm 0.10$ , Mishenina et al. (2002) derived  $[\text{Zn}/\text{Fe}] = +0.09 \pm 0.11$ , Nissen et al. (2007) derived  $[\text{Zn}/\text{Fe}] = +0.06 \pm 0.06$ , and Bensby et al. (2014) derived  $[\text{Zn}/\text{Fe}] = +0.11 \pm 0.27$ . We are aware of one additional derivation of the [Zn/Fe] ratio in HD 84937,  $+0.16 \pm 0.08$  (Sneden et al. 2016). Our result agrees with four of these five previous studies, so we are not concerned about the [Zn/Fe] ratio in HD 84937.

We noted in Section 1 the discrepancy between the non-LTE calculations of Yan et al. (2015) and Andrievsky et al. (2018) for the Cu I line at 5105 Å in HD 94028, the only line and star common to the two studies. From their tables and discussion, we infer non-LTE  $\log \epsilon(\text{Cu})$  abundances of 2.37 (Yan et al.) and 2.63 (Andrievsky et al.) for this line. Our  $\log \epsilon$  abundance inferred from the four Cu II lines in HD 94028 is 2.34, which favors the Yan et al. value. Further evaluation of the two sets of non-LTE calculations must await the availability of additional lines in more stars in common.

Four previous studies have also examined Cu II or Zn II lines in one or two stars each per study. Roederer & Lawler (2012) derived [Cu II/Fe] and [Zn II/Fe] in HD 160617, Roederer (2012) derived [Zn II/Fe] in HD 94028 and HD 140283, Roederer et al. (2016a) reanalyzed both [Cu II/Fe] and [Zn II/Fe] in HD 94028, and Andrievsky et al. (2018) derived [Cu II/Fe] in HD 84937 and HD 140283. Our ratios agree in all cases with those derived by previous analyses within their mutual  $1\sigma$  uncertainties. The same STIS spectra were used in all of these studies, so it is reassuring that there is good agreement.

## 5. DISCUSSION

### 5.1. Copper

Figure 3 illustrates the Cu abundances derived in this study. The top panel of Figure 3 compares the [Cu/Fe] ratios derived from neutral lines with a representative selection of previous studies from the litera-

ture. The references are listed in the caption to Figure 3. We make no attempt to distinguish among stars in different Galactic components or to correct for differences in the atomic data or lines used by different authors. For consistency with the present sample, only relatively warm ( $T_{\text{eff}} > 5600$  K) subgiant or main sequence stars are included. Our derived [Cu/Fe] ratios trace the trends found in metal-poor stars in the Solar neighborhood, as revealed by previous studies. There is a plateau at  $[\text{Cu}/\text{Fe}] = -0.92 \pm 0.04$  for the four stars in our sample with  $[\text{Fe}/\text{H}] < -1.8$ , a gradual increase of [Cu/Fe] with increasing metallicity, and another plateau at  $[\text{Cu}/\text{Fe}] \approx -0.1$  for comparison stars with  $[\text{Fe}/\text{H}] > -0.8$ .

The middle panel of Figure 3 illustrates the [Cu/Fe] ratios derived from singly-ionized lines. The overall trend among stars with  $[\text{Fe}/\text{H}] \lesssim -1$  is shifted up by a few tenths of a dex relative to the trend found when using neutral lines. The [Cu/Fe] ratios remain sub-Solar in the lowest metallicity stars, and the plateau, if such a description is appropriate, is found at  $[\text{Cu}/\text{Fe}] = -0.60 \pm 0.05$  for the four stars in our sample with  $[\text{Fe}/\text{H}] < -1.8$ . The trend of increasing [Cu/Fe] with increasing metallicity remains, although the magnitude of the slope is reduced. The [Cu/Fe] ratio in the most metal-rich star in our sample, HD 76932, remains consistent with the Solar ratio.

The bottom panel of Figure 3 shows two sets of values on the same axes, and we propose that these two quantities probe the same effect. The black squares show the difference ( $\Delta$ ) between the [Cu/H] ratios derived from ionized lines and neutral lines in our study. The magnitude of the difference is greatest in the lowest metallicity stars ( $+0.36 \pm 0.06$  dex), and it decreases toward higher metallicities. We interpret the difference shown in the bottom panel as evidence of the over-ionization of neutral Cu in warm, metal-poor stars, which leads to an under-prediction of the Cu abundance in LTE. The open diamonds and circles in the bottom panel of Figure 3 show the theoretical non-LTE corrections for Cu I lines calculated by Yan et al. (2015) and Andrievsky et al. (2018). The sign and magnitude of the non-LTE corrections generally match our empirical measurements of the differences between abundances derived from Cu II and Cu I lines, although the Andrievsky et al. non-LTE calculations predict slightly larger corrections at the lowest metallicities studied. We are encouraged by the overall agreement, and we propose that these observational signatures generally validate the theoretical calculations for warm stars by Yan et al. and Andrievsky et al.

### 5.2. Zinc

Figure 4 illustrates the our derived [Zn/Fe] ratios. A representative selection of [Zn/Fe] ratios from previous studies of warm, metal-poor stars is shown for comparison. The top panel shows the ratios derived from neutral lines. The six stars in our sample exhibit a consistent

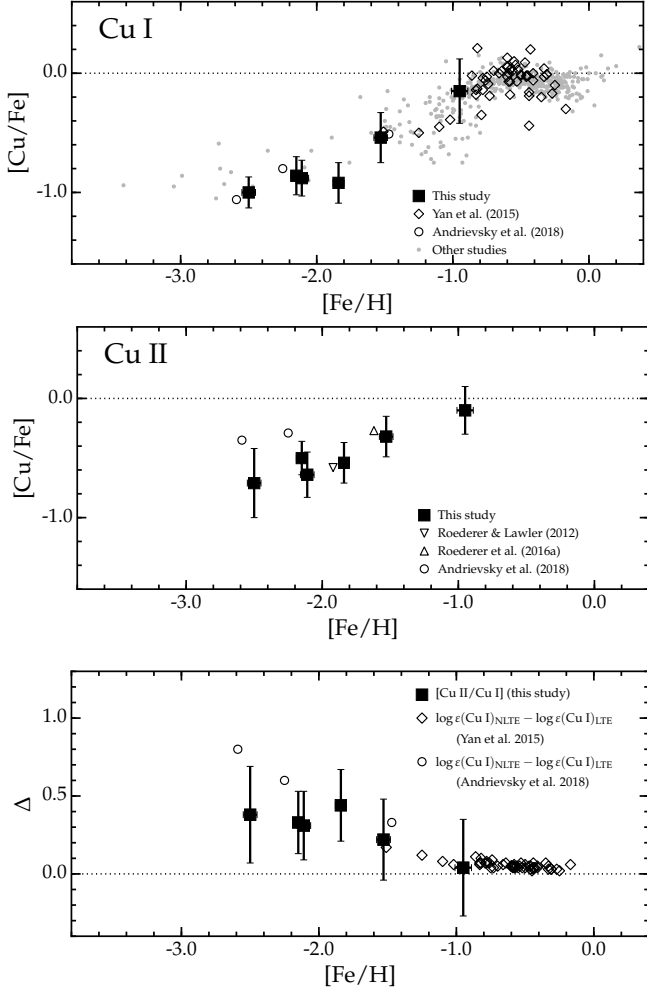


**Figure 3.** Derived Cu abundances. The top panel shows  $[\text{Cu}/\text{Fe}]$  derived from Cu I and Fe I lines for the stars in our sample, which are designated by filled squares. The samples of Yan et al. (2015) and Andrievsky et al. (2018) are designated by open diamonds and circles. A representative selection of other literature studies of disk and halo stars is designated by small gray circles. These data are drawn from Sneden et al. (1991), Mishenina & Kovtyukh (2001); Mishenina et al. (2002), Reddy et al. (2003, 2006), Bihain et al. (2004), Lai et al. (2008), Nissen & Schuster (2011), and Ishigaki et al. (2013). The middle panel shows  $[\text{Cu}/\text{Fe}]$  derived from Cu II and Fe II lines for the stars in our sample. Two stars analyzed by Andrievsky et al., one star analyzed by Roederer & Lawler (2012), and one star analyzed by Roederer et al. (2016a) are also shown. The bottom panel compares our  $[\text{Cu II}/\text{Cu I}]$  ratios with the Cu I non-LTE corrections presented by Yan et al. and Andrievsky et al. Note that the  $[\text{Cu II}/\text{Cu I}]$  ratios in the bottom panel are calculated from the  $[\text{Cu}/\text{H}]$  ratios, so they are not a simple difference of the  $[\text{Cu}/\text{Fe}]$  ratios shown in the top panels. The dotted line in all panels represents the Solar  $[\text{Cu}/\text{Fe}]$  ratio.

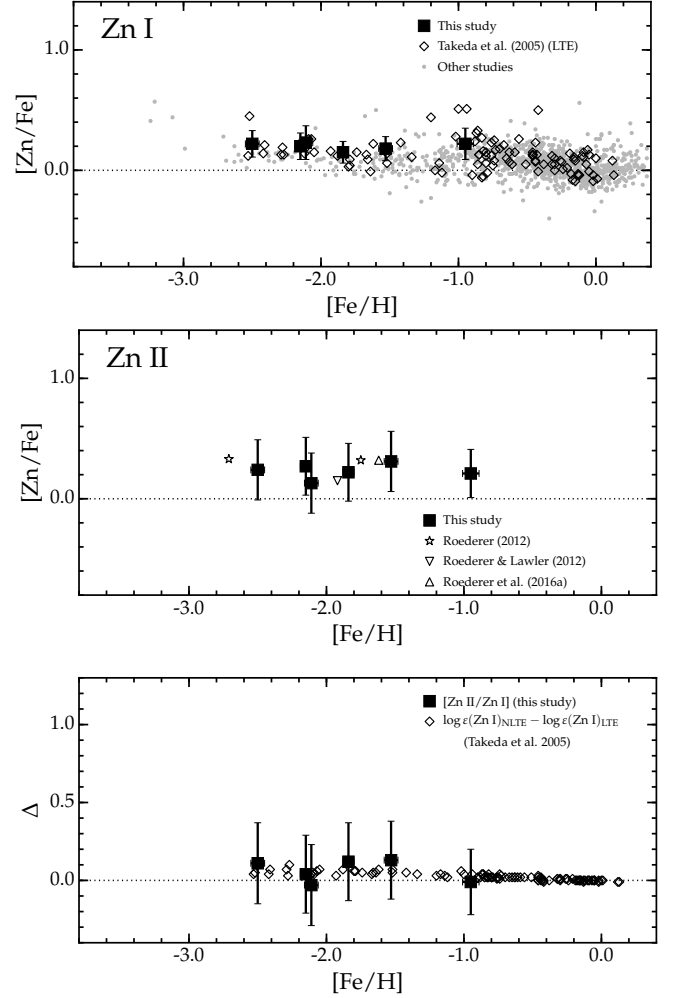


**Figure 4.** Derived Zn abundances. The top panel shows  $[\text{Zn}/\text{Fe}]$  derived from Zn I and Fe I lines for the stars in our sample, which are designated by filled squares. The sample reanalyzed by Takeda et al. (2005) is designated by open diamonds. A representative selection of other literature studies of disk and halo stars is designated by small gray circles. These data are drawn from Sneden et al. (1991), Mishenina & Kovtyukh (2001), Mishenina et al. (2002), Reddy et al. (2003, 2006), Bihain et al. (2004), Nissen et al. (2007), Lai et al. (2008), Nissen & Schuster (2011), Ishigaki et al. (2013), and Bensby et al. (2014). The middle panel shows  $[\text{Zn}/\text{Fe}]$  derived from Zn II and Fe II lines for the stars in our sample. Three stars (re)analyzed by Roederer (2012), Roederer & Lawler (2012), and Roederer et al. (2016a) are also shown. The bottom panel compares our  $[\text{Zn II}/\text{Zn I}]$  ratios with the Zn I non-LTE corrections presented by Takeda et al. Note that the  $[\text{Zn II}/\text{Zn I}]$  ratios in the bottom panel are calculated from the  $[\text{Zn}/\text{H}]$  ratios, so they are not a simple difference of the  $[\text{Zn}/\text{Fe}]$  ratios shown in the top panels. The dotted line in all panels represents the Solar  $[\text{Zn}/\text{Fe}]$  ratio.

enhancement of  $[Zn/Fe] = +0.19 \pm 0.02$ . As in the case of Cu, the stars in our sample outline the general trends found in the stars with similar metallicity in the comparison samples.

The middle panel of Figure 4 shows the  $[Zn/Fe]$  ratios derived from ionized lines. The mean  $[Zn/Fe]$  ratio is  $+0.23 \pm 0.04$ . No trends with metallicity are apparent, and the results are in good agreement with previous work.

The black squares in the bottom panel of Figure 4 mark the difference ( $\Delta$ ) between the  $[Zn/H]$  ratios derived from ionized lines and neutral lines in our study. The mildly enhanced  $[Zn \text{ II}/Zn \text{ I}]$  ratios found in this study are not significant in any given star. Considering all six stars as representatives of a single population, if such a simplification is appropriate, yields a mean  $[Zn \text{ II}/Zn \text{ I}]$  ratio of  $+0.06 \pm 0.04$  dex, which is also not significant. The overall good agreement in the mean offsets may suggest that our uncertainty estimates are too conservative. The open diamonds in the bottom panel of Figure 4 mark Zn I non-LTE corrections from Takeda et al. (2005). The non-LTE effects in Zn I are predicted to be small,  $< 0.1$  dex, and match the differences found by our study.

The agreement between these two quantities is perhaps not surprising. The first ionization potential of Zn is 9.39 eV, approximately 1.5 eV higher than the next-highest Fe-group element (Fe, 7.90 eV; Morton 2003), and considerably higher than the first ionization potential of Cu (7.73 eV). A substantial fraction of Zn atoms in the atmospheres of these warm stars is expected to remain neutral ( $\approx 5\text{--}50\%$ ; Roederer & Lawler 2012; Sneden et al. 2016), in contrast to other Fe-group elements ( $\sim 0.1\text{--}5\%$ ; Sneden et al.). Any over-ionization of neutral Zn has less impact on the derived abundances. Photon pumping, the bound-bound equivalent of over-ionization, has been shown to have a notable impact on the level populations of UV resonance Fe II lines (Cram et al. 1980; Shchukina et al. 2005). If a similar effect occurs for the Zn II UV resonance lines, it would exacerbate the good agreement in abundances derived from Zn I and II lines. We conclude that any such photon pumping in the Zn II resonance line at 2062 Å is minimal.

### 5.3. HD 84937: a Complete Census of Fe-Group Elements from Majority Species

Sneden et al. (2016) derived abundances for Sc through Ni from 1,158 lines of neutral and singly-ionized species (except for Sc I, for which no lines were available) in UV and optical spectra of HD 84937, which is among the UV-brightest metal-poor stars in the sky. One of the key results of that study was that LTE abundance calculations for most lines of neutral and ionized species yielded statistically identical results for all elements from Ti ( $Z = 22$ ) to Ni ( $Z = 28$ ). This implies that deviations from LTE cannot be too large among the

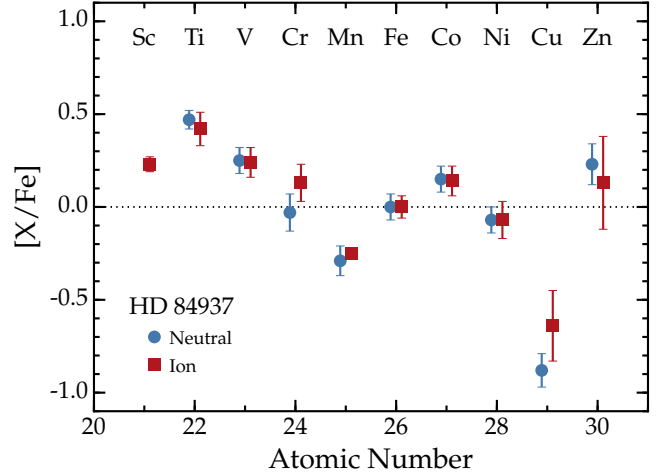


**Figure 5.** Comparison of  $[X/Fe]$  ratios for elements in the Fe group of HD 84937. The blue circles indicate ratios derived from lines of neutral species, and the red squares indicate ratios derived from lines of singly-ionized species. The data from Sc to Ni are taken from Sneden et al. (2016), and the data for Cu and Zn are derived in the present study. The dotted line marks the Solar ratio.

Fe-group elements in the atmosphere of HD 84937 and presumably other stars with similar stellar parameters and metallicity.

Sneden et al. (2016) also derived  $[Cu/Fe]$  and  $[Zn/Fe]$  from neutral species only, because no spectrum covering the Cu II and Zn II lines was available at the time. The combined results of Sneden et al. and our work are shown in Figure 5. To the best of our knowledge, HD 84937 is the first metal-poor star whose complete Fe-group ( $21 \leq Z \leq 30$ ) pattern has been derived from the majority (i.e., singly ionized) species of each element.

Our results extend this good agreement to Zn. The  $[Zn/Fe]$  ratio derived from 4 neutral lines is determined to a precision of 0.14 dex. The large abundance uncertainty, 0.25 dex, associated with a single, saturated UV resonance line of Zn II could mask moderate deviations from LTE. There is no evidence, however, for deviations larger than  $\approx 0.1$  dex at present.

Cu is the exception to the good agreement established by other Fe-group species. However, the disagreement is only moderately significant,  $[Cu \text{ II}/Cu \text{ I}] = 0.31 \pm 0.22$  dex, and it is not apparent in Figure 5, where the Fe abundances are folded into the  $[Cu/Fe]$  ratios. The uncertainty is dominated by the statistical uncertainty in measuring Cu II lines, and it is unlikely that significantly higher S/N spectra can be obtained for HD 84937 or other stars like it in the foreseeable future. The consistent results for Cu I obtained from other metal-poor stars in our sample suggest that it is likely that LTE calculations underestimate the abundance derived from Cu I lines in HD 84937.

## 6. SUMMARY

We examine archival UV and optical spectra of six warm ( $5766 \leq T_{\text{eff}} \leq 6427$  K), metal-poor ( $-2.50 \leq [\text{Fe}/\text{H}] \leq -0.95$ ) dwarf and subgiant ( $3.64 \leq \log g \leq 4.44$ ) stars. We analyze optical and UV lines from the neutral and singly-ionized species of Fe, Cu, and Zn to assess the differences that may result from over-ionization of the minority neutral species in the atmospheres of these stars.

We conclude that Cu abundances derived from Cu I lines in warm, metal-poor stars may be underestimated by  $\approx 0.36 \pm 0.06$  dex at the lowest metallicities,  $[\text{Fe}/\text{H}] < -1.8$ . At higher metallicities the magnitude of the effect lessens. Previous theoretical work by Yan et al. (2015) and Andrievsky et al. (2018) suggests this underestimation is caused by the non-LTE over-ionization of neutral Cu. Our results validate those calculations, although the Andrievsky et al. calculations may slightly overestimate the magnitude of the non-LTE corrections at the lowest metallicities. Additional observational comparisons would help clarify this matter.

Abundances derived from Zn II and Zn I differ by only  $0.06 \pm 0.04$  dex on average, which is not significant. A substantial fraction of neutral Zn is present, unlike in the case of Cu, minimizing the impact of any over-ionization of Zn. These results affirm the non-LTE calculations of Takeda et al. (2005), which predict only small non-LTE corrections for Zn I. Thus LTE abundances derived from optical Zn I lines are essentially correct to better than 0.1 dex.

Our analysis of Cu II and Zn II lines in the metal-poor ( $[\text{Fe}/\text{H}] = -2.15$ ) turnoff star HD 84937 complements the extensive work of Sneden et al. (2016) to provide a complete set of abundances for all Fe-group elements (Sc through Zn) derived from the majority singly-ionized species. The abundances derived from lines of neutral and singly-ionized species in HD 84937 moderately disagree for only one element, Cu. Roederer et al. (2018) have begun to extend this approach on six additional

stars, including several analyzed in the present study. We cannot understate the importance of access to a high-resolution UV echelle spectrograph in space for this work.

We thank the referee for offering helpful suggestions that have improved this manuscript. IUR thanks U. Heiter for discussing results in advance of publication. Generous support for Program AR-15051 has been provided by a grant from STScI, which is operated by AURA, under NASA contract NAS5-26555. IUR also acknowledges partial support from grant PHY 14-30152 (Physics Frontier Center/JINA-CEE) awarded by the U.S. National Science Foundation (NSF). PSB received financial support from the Swedish Research Council and the project grant ‘‘The New Milky Way’’ from the Knut and Alice Wallenberg Foundation. This research has made use of NASA’s Astrophysics Data System Bibliographic Services; the arXiv pre-print server operated by Cornell University; the SIMBAD and VizieR databases hosted by the Strasbourg Astronomical Data Center; the ASD hosted by NIST; the MAST at STScI; and IRAF software packages distributed by the National Optical Astronomy Observatories, which are operated by AURA, under cooperative agreement with the NSF. This work has also made use of data from the European Space Agency (ESA) mission *Gaia* (<http://www.cosmos.esa.int/gaia>), processed by the *Gaia* Data Processing and Analysis Consortium (DPAC, <http://www.cosmos.esa.int/web/gaia/dpac/consortium>). Funding for the DPAC has been provided by national institutions, in particular the institutions participating in the *Gaia* Multilateral Agreement.

*Facility:* ESO:3.6m (HARPS), HST (STIS), Keck I (HIRES), Smith (Tull), VLT (UVES)

*Software:* IRAF (Tody 1993), matplotlib (Hunter 2007), MOOG (Sneden 1973), numpy (van der Walt et al. 2011), R (R Core Team 2014), scipy (Jones et al. 2001)

## REFERENCES

- Akerman, C. J., Ellison, S. L., Pettini, M., & Steidel, C. C. 2005, *A&A*, 440, 499
- Alonso, A., Arribas, S., & Martínez-Roger, C. 1999, *A&AS*, 140, 261
- Andrievsky, S., Bonifacio, P., Caffau, E., et al. 2018, *MNRAS*, 473, 3377
- Anstee, S. D., & O’Mara, B. J. 1991, *MNRAS*, 253, 549
- Anstee, S. D., & O’Mara, B. J. 1995, *MNRAS*, 276, 859
- Asplund, M., Grevesse, N., Sauval, A. J., & Scott, P. 2009, *ARA&A*, 47, 481
- Barklem, P. S., & O’Mara, B. J. 1997, *MNRAS*, 290, 102
- Barklem, P. S., & O’Mara, B. J. 1998, *MNRAS*, 300, 863
- Barklem, P. S., & O’Mara, B. J. 2000, *MNRAS*, 311, 535
- Barklem, P. S., & Aspelund-Johansson, J. 2005, *A&A*, 435, 373
- Barklem, P. S., Piskunov, N., & O’Mara, B. J. 2000, *A&AS*, 142, 467
- Barklem, P. S., Christlieb, N., Beers, T. C., et al. 2005, *A&A*, 439, 129
- Bensby, T., Feltzing, S., & Oey, M. S. 2014, *A&A*, 562, A71
- Bergeson, S. D., & Lawler, J. E. 1993, *ApJ*, 408, 382
- Bergemann, M., Lind, K., Collet, R., Magic, Z., & Asplund, M. 2012, *MNRAS*, 427, 27

- Bihain, G., Israelian, G., Rebolo, R., Bonifacio, P., & Molaro, P. 2004, *A&A*, 423, 777
- Bonifacio, P., Caffau, E., & Ludwig, H.-G. 2010, *A&A*, 524, A96
- Casagrande, L., Ramírez, I., Meléndez, J., Bessell, M., & Asplund, M. 2010, *A&A*, 512, A54
- Casagrande, L., Schönrich, R., Asplund, M., et al. 2011, *A&A*, 530, A138
- Casagrande, L., & VandenBerg, D. A. 2014, *MNRAS*, 444, 392
- Castelli, F., Kurucz, R. L. Proc. IAU Symp. No 210, Modelling of Stellar Atmospheres, N. Piskunov et al., eds. 2003, A20
- Cayrel, R., Depagne, E., Spite, M., et al. 2004, *A&A*, 416, 1117
- Cescutti, G., Matteucci, F., François, P., & Chiappini, C. 2007, *A&A*, 462, 943
- Cohen, J. G., Christlieb, N., McWilliam, A., et al. 2008, *ApJ*, 672, 320-341
- Cohen, J. G., Christlieb, N., Thompson, I., et al. 2013, *ApJ*, 778, 56
- Cram, L. E., Lites, B. W., & Rutten, R. J. 1980, *ApJ*, 241, 374
- Cutri, R. M., Skrutskie, M. F., van Dyk, S., et al. 2003, VizieR Online Data Catalog: 2MASS All-Sky Catalog of Point Sources, 2246, 0
- Dekker, H., D’Odorico, S., Kaufer, A., Delabre, B., & Kotzłowski, H. 2000, Proc. SPIE, 4008, 534
- Den Hartog, E. A., Ruffoni, M. P., Lawler, J. E., et al. 2014, *ApJS*, 215, 23
- Ducati, J. R. 2002, VizieR Online Data Catalog: Catalogue of Stellar Photometry in Johnson’s 11-color System, 2237, 0
- Elbel, M., Fischer, W., & Hartmann, M. 1963, *Zeitschrift für Physik*, 176, 288
- Elbel, M. & Hühnermann, H. 1969, *J. Phys. (Paris) Colloques*, 30, C1-41
- Fedchak, J. A., & Lawler, J. E. 1999, *ApJ*, 523, 734
- François, P., Matteucci, F., Cayrel, R., et al. 2004, *A&A*, 421, 613
- Gaia Collaboration, Brown, A. G. A., Vallenari, A., et al. 2016, *A&A*, 595, A2
- Goswami, A., & Prantzos, N. 2000, *A&A*, 359, 191
- Hirai, Y., Saitoh, T. R., Ishimaru, Y., & Wanajo, S. 2018, *ApJ*, 855, 63
- Hollek, J. K., Frebel, A., Roederer, I. U., et al. 2011, *ApJ*, 742, 54
- Hunter, J.D. 2011, *Computing in Science & Engineering*, 9, 90
- Ishigaki, M. N., Aoki, W., & Chiba, M. 2013, *ApJ*, 771, 67
- Jacobson, H. R., Keller, S., Frebel, A., et al. 2015, *ApJ*, 807, 171
- Jones, E., Oliphant, E., Peterson, P., et al. 2001, *SciPy: Open Source Scientific Tools for Python*, <http://www.scipy.org>
- Kimble, R. A., Woodgate, B. E., Bowers, C. W., et al. 1998, *ApJL*, 492, L83
- Kobayashi, C., Umeda, H., Nomoto, K., Tominaga, N., & Ohkubo, T. 2006, *ApJ*, 653, 1145
- Kramida, A., Nave, G., & Reader, J. 2017a, *Atoms*, 5, 9
- Kramida, A., Ralchenko, Y., Reader, J., and the NIST ASD Team. 2017b, *NIST Atomic Spectra Database (v. 5.5.1)*, online, URL: <http://physics.nist.gov/asd>
- Kurucz, R. L. 2011, *Canadian Journal of Physics*, 89, 417
- Lai, D. K., Bolte, M., Johnson, J. A., et al. 2008, *ApJ*, 681, 1524-1556
- Lawler, J. E., Sneden, C., Cowan, J. J., Ivans, I. I., & Den Hartog, E. A. 2009, *ApJS*, 182, 51
- Lawler, J. E., Sneden, C., Cowan, J. J., Den Hartog, E. A., & Wood, M. P. 2017, *Canadian Journal of Physics*, 95, 783
- Mashonkina, L., Gehren, T., Shi, J.-R., Korn, A. J., & Grupp, F. 2011, *A&A*, 528, A87
- Mayor, M., Pepe, F., Queloz, D., et al. 2003, *The Messenger*, 114, 20
- McCall, M. L. 2004, *AJ*, 128, 2144
- Meléndez, J., & Barbuy, B. 2009, *A&A*, 497, 611
- Meléndez, J., Casagrande, L., Ramírez, I., Asplund, M., & Schuster, W. J. 2010, *A&A*, 515, L3
- Mishenina, T. V., & Kovtyukh, V. V. 2001, *A&A*, 370, 951
- Mishenina, T. V., Kovtyukh, V. V., Soubiran, C., Travaglio, C., & Busso, M. 2002, *A&A*, 396, 189
- Morton, D. C. 2003, *ApJS*, 149, 205
- Munari, U., Henden, A., Frigo, A., et al. 2014, *AJ*, 148, 81
- Nissen, P. E., & Schuster, W. J. 2010, *A&A*, 511, L10
- Nissen, P. E., & Schuster, W. J. 2011, *A&A*, 530, A15
- Nissen, P. E., Akerman, C., Asplund, M., et al. 2007, *A&A*, 469, 319
- O’Brian, T. R., Wickliffe, M. E., Lawler, J. E., Whaling, W., & Brault, J. W. 1991, *Journal of the Optical Society of America B Optical Physics*, 8, 1185
- Paunzen, E. 2015, *A&A*, 580, A23
- Pettini, M., Smith, L. J., Hunstead, R. W., & King, D. L. 1994, *ApJ*, 426, 79
- Prochaska, J. X., & Wolfe, A. M. 1999, *ApJS*, 121, 369
- R Core Team, 2014, “R: A Language and Environment for Statistical Computing,” R Foundation for Statistical Computing, Vienna, Austria. URL <http://www.R-project.org>

- Rafelski, M., Wolfe, A. M., Prochaska, J. X., Neeleman, M., & Mendez, A. J. 2012, *ApJ*, 755, 89
- Ramírez, I., & Meléndez, J. 2005, *ApJ*, 626, 465
- Reddy, B. E., Tomkin, J., Lambert, D. L., & Allende Prieto, C. 2003, *MNRAS*, 340, 304
- Reddy, B. E., Lambert, D. L., & Allende Prieto, C. 2006, *MNRAS*, 367, 1329
- Reggiani, H., Meléndez, J., Kobayashi, C., Karakas, A., & Placco, V. 2017, *A&A*, 608, A46
- Roederer, I. U. 2012, *ApJ*, 756, 36
- Roederer, I. U., & Lawler, J. E. 2012, *ApJ*, 750, 76
- Roederer, I. U., Cowan, J. J., Karakas, A. I., et al. 2010, *ApJ*, 724, 975
- Roederer, I. U., Preston, G. W., Thompson, I. B., et al. 2014a, *AJ*, 147, 136
- Roederer, I. U., Schatz, H., Lawler, J. E., et al. 2014b, *ApJ*, 791, 32
- Roederer, I. U., Karakas, A. I., Pignatari, M., & Herwig, F. 2016a, *ApJ*, 821, 37
- Roederer, I. U., Placco, V. M., & Beers, T. C. 2016b, *ApJL*, 824, L19
- Roederer, I. U., Sneden, C., Lawler, J. E., et al. 2018, *AAS Journals*, submitted
- Romano, D., & Matteucci, F. 2007, *MNRAS*, 378, L59
- Ruffoni, M. P., Den Hartog, E. A., Lawler, J. E., et al. 2014, *MNRAS*, 441, 3127
- Saito, Y.-J., Takada-Hidai, M., Honda, S., & Takeda, Y. 2009, *PASJ*, 61, 549
- Shchukina, N. G., Trujillo Bueno, J., & Asplund, M. 2005, *ApJ*, 618, 939
- Shi, J. R., Gehren, T., Zeng, J. L., Mashonkina, L., & Zhao, G. 2014, *ApJ*, 782, 80
- Sitnova, T., Zhao, G., Mashonkina, L., et al. 2015, *ApJ*, 808, 148
- Sneden, C.A. 1973, Ph.D. thesis, University of Texas at Austin
- Sneden, C., Gratton, R. G., & Crocker, D. A. 1991, *A&A*, 246, 354
- Sneden, C., Cowan, J. J., Kobayashi, C., et al. 2016, *ApJ*, 817, 53
- Sobeck, J. S., Primas, F., Sneden, C., & Ivans, I. I. 2008, *AIP Conf. Proc.* “First Stars III,” 990, 187
- Sobeck, J. S., Kraft, R. P., Sneden, C., et al. 2011, *AJ*, 141, 175
- Takeda, Y., Hashimoto, O., Taguchi, H., et al. 2005, *PASJ*, 57, 751
- Timmes, F. X., Woosley, S. E., & Weaver, T. A. 1995, *ApJS*, 98, 617
- Tody, D. 1993, *Astronomical Data Analysis Software and Systems II*, 52, 173
- Tull, R. G., MacQueen, P. J., Sneden, C., & Lambert, D. L. 1995, *PASP*, 107, 251
- Unsöld, A., *Physik der Sternatmosphären*, Springer-Verlag, Berlin, 1955, p. 332
- van der Walt, S., Colbert, S. C., Varoquaux, G. 2011, *Computing in Science & Engineering*, 13, 22
- van Leeuwen, F. 2007, *A&A*, 474, 653
- Vogt, S. S., Allen, S. L., Bigelow, B. C., et al. 1994, *Proc. SPIE*, 2198, 362
- Woodgate, B. E., Kimble, R. A., Bowers, C. W., et al. 1998, *PASP*, 110, 1183
- Yan, H. L., Shi, J. R., & Zhao, G. 2015, *ApJ*, 802, 36
- Yan, H. L., Shi, J. R., Nissen, P. E., & Zhao, G. 2016, *A&A*, 585, A102